IEEE Photonics Journal
An IEEE Photonics Society Publication

Open Access

Microwave Photonic Image-Reject Mixer Based on a Tunable Microwave Photonic Filter With High Rejection

Volume 10, Number 6, December 2018

Xi Kong
Yuan Yu
Haitao Tang
Xinliang Zhang

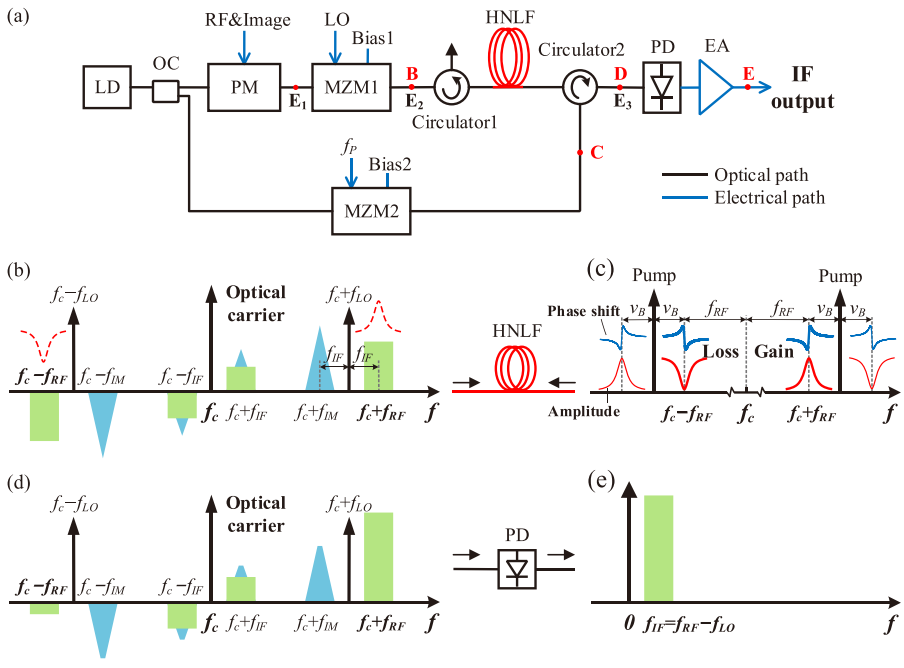

DOI: 10.1109/JPHOT.2018.2883113
1943-0655 © 2018 IEEE

IEEE photonics SOCIETY

IEEE

Microwave Photonic Image-Reject Mixer Based on a Tunable Microwave Photonic Filter With High Rejection

Xi Kong, Yuan Yu, Haitao Tang, and Xinliang Zhang

Wuhan National Laboratory for Optoelectronics and the School of Optical and Electrical Information, Huazhong University of Science and Technology, Wuhan 430074, China

DOI:10.1109/JPHOT.2018.2883113

Manuscript received November 3, 2018; revised November 16, 2018; accepted November 20, 2018. Date of publication November 23, 2018; date of current version December 7, 2018. This work was supported in part by the National Natural Science Foundation of China under Grants 61501194 and 11664009, in part by Hubei Provincial Natural Science Foundation of China under Grants 2014CFA004, 2015CFB231, and 2016CFB370, in part by the Fundamental Research Funds for the Central Universities (HUST: 2016YXMS025), and in part by the Director Fund of WNLO. Corresponding author: Y. Yu (e-mail: yuan_yu@hust.edu.cn).

Abstract: In a heterodyne receiver, the image can interfere with the desired signal and must be eliminated at the mixing stage. This paper presents a flexible microwave photonic image-reject mixer based on a widely tunable microwave photonic filter (MPF), which is used to select the desired signal and suppress the image. The MPF is realized by using stimulated Brillouin scattering, which offers significant advantages of wideband tunability, high selectivity, and large image rejection. In this work, a theoretical model is established to describe the operation principle of the proposed mixer at first. Then, in the experiment, a 7.8-GHz radio frequency (RF) signal is successfully down-converted to an intermediate frequency signal between 0.2 and 1.5 GHz, with an image rejection of larger than 40 dB. Additionally, when the RF frequency is tuned from 1.8 to 19.8 GHz, the image rejection remains above 40 dB.

Index Terms: Microwave photonics, image-reject mixer (IRM), microwave photonic filter (MPF), stimulated Brillouin scattering (SBS).

1. Introduction

The microwave mixer, which is used to convert the frequency of the microwave signal, is conventionally achieved by electrical techniques [1]. With the development of photonic techniques, the microwave photonic mixer has attracted great interest for its inherent advantages, such as large bandwidth, high isolation, parallel processing capacity, and immunity to electro-magnetic interference [2]–[4]. So far, several microwave photonic mixers have been proposed and demonstrated. A basic microwave photonic mixer is implemented by using external modulation and heterodyne detection [2]. In order to improve the conversion efficiency, microwave photonic mixers based on optical carrier suppression [5], cross gain modulation [6], and cross phase modulation [7] are developed. Additionally, a full-duplex system for downlink and uplink have been reported [8]. However, in practical applications, these microwave photonic mixers cannot reject the interference from the image frequency. The image problem can be described as follows: When the received radio frequency (RF) signals are mixed with the local oscillator (LO) f_{LO}, the desired RF signal at frequency

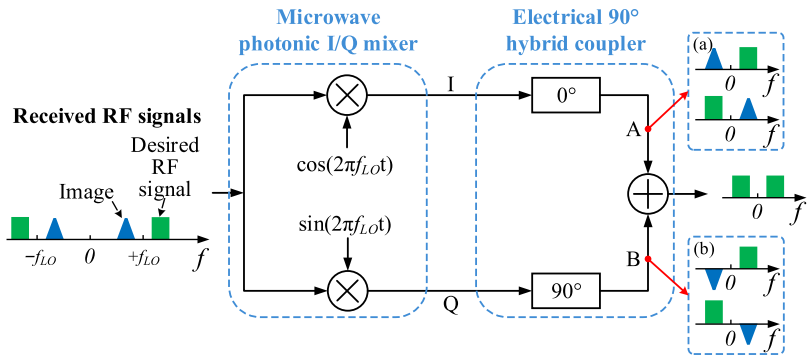

Fig. 1. Hartley architecture. Electrical spectra at points (a) A and (b) B. I/Q: in-phase/quadrature.

$f_{RF} = f_{LO} + f_{IF}$ and the image at frequency $f_{IM} = f_{LO} - f_{IF}$ are simultaneously down-converted to the same intermediate frequency (IF) f_{IF} band, thus an interference from the image is generated [1].

To eliminate the image, microwave photonic image-reject mixer is developed [9]–[14], [16], [17]. A commonly used configuration for microwave photonic image-reject mixer is Hartley architecture [9]–[14]. As illustrated in Fig. 1, the received RF signals are split into two paths and mixed with the quadrature LO. Then, the IF signals down-converted from the received RF signals are fed into an electrical 90° hybrid coupler. Fig. 1(a) and (b) show the electrical spectra at points A and B, respectively. As can be seen, the IF signals down-converted from the desired RF signals are in phase while the IF components down-converted from the images are in antiphase. Therefore, the summed IF outputs are free from the image. The key to Hartley architecture is microwave photonic in-phase/quadrature (I/Q) mixing. In general, an electrical 90° hybrid coupler can be used to generate the quadrature LO [9] or RF [10] inputs. However, an electrical 90° hybrid coupler cannot cover a wide RF frequency range with precise 90° phase difference, which limits the RF frequency range of the image-reject mixer. Recently, it has been suggested to introduce a precise 90° phase difference to I/Q paths by microwave photonic phase shifter, which can be achieved by using a dual-polarization dual-drive Mach-Zehnder modulator (MZM) [11], a dual-parallel MZM [12], a polarization modulator together with two polarization controllers (PCs) [13], or an optical 90° hybrid coupler [14]. However, if the image rejection across a low RF band is required in [11]–[14], an optical filter with sharp passband skirts is certainly needed to select the useful optical sidebands. In addition, these microwave photonic image-reject mixers based on Hartley architecture are sensitive to phase and amplitude imbalance [15]. Alternatively, an electrical filter can be used to pre-select the desired RF signal and suppress the image, and an image rejection of better than 60 dB are achieved [16], [17]. However, the electrical filters used in [16] and [17] are not adjustable, and a two-stage mixing must be adopted to remove the image and convert the desired RF signal to an IF signal.

In this paper, we propose a flexible microwave photonic image-reject mixer based on a microwave photonic filter (MPF), which is realized by using stimulated Brillouin scattering (SBS). Thanks to the advantages of the SBS-based MPF, including continuous wideband tunability, high resolution and high out-of-band rejection [18]–[20], the image can be exactly and greatly rejected by properly tuning the central frequency of the MPF. The theoretical model of the proposed microwave photonic image-reject mixer is established, and both simulations and experiments are carried out to demonstrate the proposed scheme. In experiment, a 7.8-GHz desired RF signal is successfully down-converted to an IF signal within 0.2 and 1.5 GHz, and the image rejection exceeds 40 dB. The image rejection across a wide RF band of 1.8–19.8 GHz is also demonstrated.

2. Operation Principle

The operation principle of the proposed microwave photonic image-reject mixer is shown in Fig. 2. In Fig. 2(a), a continuous wave (CW) light emitted from a laser diode (LD) is split into two paths via a

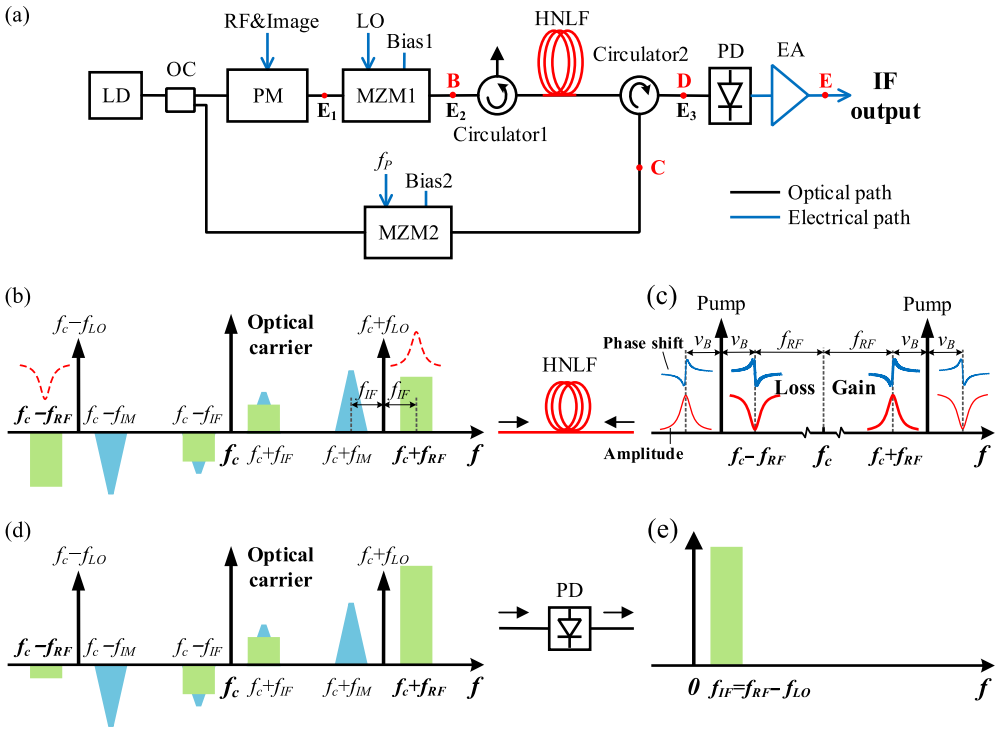

Fig. 2. Operation principle of the proposed microwave photonic image-reject mixer. (a) Schematic diagram. Optical spectra at points (b) B, (c) C, and (d) D. (e) Electrical spectra at point E. LD: laser diode; OC: optical coupler; PM: phase modulator; RF: radio frequency; MZM: Mach-Zehnder modulator; HNLF: high-nonlinear fiber; LO: local oscillator; PD: photodetector; EA: electrical amplifier; IF: intermediate frequency; SBS: stimulated Brillouin scattering.

50:50 optical coupler (OC). In the upper path, the CW light is first injected into the phase modulator (PM), which is driven by the desired RF signal and the image. For small signal modulation, the electric field at the output of the PM can be approximated as

$$E_1(t) = \sqrt{P_{in}t_1}\exp(j2\pi f_c t) \times [J_0(m_{RF}) + jJ_1(m_{RF})\exp(j2\pi f_{RF}t) + jJ_1(m_{RF})\exp(-j2\pi f_{RF}t)] \times [J_0(m_{IM}) + jJ_1(m_{IM})\exp(j2\pi f_{IM}t) + jJ_1(m_{IM})\exp(-j2\pi f_{IM}t)], \quad (1)$$

where f_c is the frequency of the CW light, P_{in} is the optical power injected into the PM, t_1 is the optical insertion loss of the PM, $J_n(\blacksquare)$ denotes the nth-order Bessel function of the first kind with $n = 0$ and 1, f_{RF} and $m_{RF} = \pi V_{RF}/V_{\pi 1}$ are the frequency and modulation index of the desired RF signal respectively, f_{IM} and $m_{IM} = \pi V_{IM}/V_{\pi 1}$ are the frequency and modulation index of the image respectively, V_{RF} and V_{IM} are the amplitudes of the desired RF signal and image respectively, $V_{\pi 1}$ denotes the half-wave voltage of the PM.

The phase-modulated optical signal is then launched into the MZM1, which is driven by the LO. Considering the components that mainly contribute to the IF output, the electric field at the output of the MZM1 is given by

$$E_2(t) = E_1(t)/2 \times \sqrt{t_2} \times [1 + \exp(j\theta)\exp(jm_{LO}\cos(2\pi f_{LO}t))]$$

$$\approx \frac{\sqrt{P_{in}t_1t_2}}{2}\exp(j2\pi f_c t) \times \{J_0(m_{RF})J_0(m_{IM})[1 + J_0(m_{LO})e^{j\theta}]$$

$$+ jJ_0(m_{RF})J_0(m_{IM})J_1(m_{LO})e^{j\theta}\left(\exp\left(j2\pi f_{LO}t\right) + \exp\left(-j2\pi f_{LO}t\right)\right)$$

$$+ jJ_0(m_{IM})J_1(m_{RF})\left[1 + J_0(m_{LO})e^{j\theta}\right]\left(\exp\left(j2\pi f_{RF}t\right) + \exp\left(-j2\pi f_{RF}t\right)\right)$$

$$+ jJ_0(m_{RF})J_1(m_{IM})\left[1 + J_0(m_{LO})e^{j\theta}\right]\left(\exp\left(j2\pi f_{IM}t\right) + \exp\left(-j2\pi f_{IM}t\right)\right)$$

$$- J_0(m_{IM})J_1(m_{RF})J_1(m_{LO})e^{j\theta}\left(\exp\left(j2\pi(f_{RF} - f_{LO})t\right) + \exp\left(-j2\pi(f_{RF} - f_{LO})t\right)\right)$$

$$- J_0(m_{RF})J_1(m_{IM})J_1(m_{LO})e^{j\theta}\left(\exp\left(j2\pi(f_{LO} - f_{IM})t\right) + \exp\left(-j2\pi(f_{LO} - f_{IM})t\right)\right)\Big\}, \tag{2}$$

where t_2 is the insertion loss of the MZM1, θ is the phase shift induced by the dc bias voltage applied to MZM1, f_{LO} and $m_{LO} = \pi V_{LO}/V_{\pi 2}$ are the frequency and modulation index of the LO respectively, V_{LO} is the amplitude of the LO, $V_{\pi 2}$ denotes the half-wave voltage of the MZM1. The terms with frequencies f_c, $f_c \pm f_{LO}$, $f_c \pm f_{RF}$, $f_c \pm f_{IM}$, $f_c \pm (f_{RF} - f_{LO})$, and $f_c \pm (f_{LO} - f_{IM})$ denote, respectively, the optical carrier, LO sidebands, desired RF signal sidebands, image sidebands, IF sidebands generated by the desired RF signal and LO, and IF sidebands generated by the image and LO, as shown in Fig. 2(b).

The phase- and intensity-modulated optical signals are then fed into a high-nonlinear fiber (HNLF) via circulator1 and interact with the counter-propagating pump light generated by applying a pump tone to MZM2 that is biased at its minimum transmission point. The frequency of the pump tone is set to

$$f_P = f_{RF} + \nu_B, \tag{3}$$

where ν_B is the Brillouin frequency shift of the HNLF. The optical spectrum of the pump light is shown in Fig. 2(c). Each sideband of the pump light introduces both SBS gain and loss spectra, where the red solid curves represent the amplitude response and the blue solid curves represent the phase shift [19]. Especially, the SBS gain spectrum generated by the +1st-order sideband of the pump light is aligned with the +1st-order sideband of the desired RF signal, and the SBS loss spectrum generated by the −1st-order sideband of the pump light is aligned with the −1st-order sideband of the desired RF signal. The pump induced SBS gain factor g and loss factor α is described as [21]

$$g(\Delta f_1) = \frac{g_0}{2}\frac{(\Gamma_B/2)^2}{\Delta f_1^2 + (\Gamma_B/2)^2} + j\frac{g_0}{4}\frac{\Gamma_B \Delta f_1}{\Delta f_1^2 + (\Gamma_B/2)^2}, \tag{4a}$$

$$\alpha(\Delta f_2) = -\frac{g_0}{2}\frac{(\Gamma_B/2)^2}{\Delta f_2^2 + (\Gamma_B/2)^2} - j\frac{g_0}{4}\frac{\Gamma_B \Delta f_2}{\Delta f_2^2 + (\Gamma_B/2)^2}, \tag{4b}$$

where g_0 and Γ_B are the line-center gain factor and Brillouin gain bandwidth of the HNLF respectively, Δf_1 is the frequency deviation from $f_c + f_{RF}$, and Δf_2 is the frequency deviation from $f_c - f_{RF}$.

We assume that the Brillouin gain is not saturated during the SBS process. As the phase- and intensity-modulated optical signals propagate along the HNLF, the +1st-order sidebands of the optical signals are exponentially amplified. Meanwhile, the −1st-order sidebands of the optical signals are exponentially attenuated [21]. After the SBS process, the electric field of the optical signals is given by

$$E_3(t) = \frac{\sqrt{P_{in}t_1t_2}}{2}e^{j2\pi f_c t} \times \left\{J_0(m_{RF})J_0(m_{IM})\left[1 + J_0(m_{LO})e^{j\theta}\right] + jJ_0(m_{RF})J_0(m_{IM})J_1(m_{LO})e^{j\theta}\right.$$
$$\left. \times \left[G(f_{LO})e^{j\varphi(f_{LO})}e^{j2\pi f_{LO}t} + A(f_{LO})e^{j\varphi(f_{LO})}e^{-j2\pi f_{LO}t}\right] + jJ_0(m_{IM})J_1(m_{RF})\left[1 + J_0(m_{LO})e^{j\theta}\right]\right.$$

$$\times \left[G(f_{RF})e^{j\varphi(f_{RF})}e^{j2\pi f_{RF}t} + A(f_{RF})e^{j\varphi(f_{RF})}e^{-j2\pi f_{RF}t}\right] + jJ_0(m_{RF})J_1(m_{IM})\left[1 + J_0(m_{LO})e^{j\theta}\right]$$
$$\times \left[G(f_{IM})e^{j\varphi(f_{IM})}e^{j2\pi f_{IM}t} + A(f_{IM})e^{j\varphi(f_{IM})}e^{-j2\pi f_{IM}t}\right] - J_0(m_{IM})J_1(m_{RF})J_1(m_{LO})e^{j\theta}$$
$$\times \left[e^{j2\pi(f_{RF}-f_{LO})t} + e^{-j2\pi(f_{RF}-f_{LO})t}\right] - J_0(m_{RF})J_1(m_{IM})J_1(m_{LO})e^{j\theta} \times \left[e^{j2\pi(f_{LO}-f_{IM})t} + e^{-j2\pi(f_{LO}-f_{IM})t}\right]\Big\}, \quad (5)$$

where $G(f)$, $A(f)$, and $\varphi(f)$ are expressed as

$$G(f) = \exp\left\{\mathrm{Re}\left[g\left((f_c + f) - (f_c + f_{RF})\right)\right] \times l_P L\right\} = e^{\frac{g_0 l_P L}{2}\frac{(\Gamma_B/2)^2}{(f-f_{RF})^2+(\Gamma_B/2)^2}}, \quad (6)$$

$$A(f) = \exp\left\{\mathrm{Re}\left[\alpha\left((f_c - f) - (f_c - f_{RF})\right)\right] \times l_P L\right\} = e^{-\frac{g_0 l_P L}{2}\frac{(\Gamma_B/2)^2}{(f-f_{RF})^2+(\Gamma_B/2)^2}}, \quad (7)$$

$$\varphi(f) = \mathrm{Im}\left\{g\left[(f_c + f) - (f_c + f_{RF})\right]\right\} \times l_P L = \mathrm{Im}\left\{\alpha\left[(f_c - f) - (f_c - f_{RF})\right]\right\} \times l_P L$$
$$= \frac{g_0 l_P L}{4}\frac{\Gamma_B(f - f_{RF})}{(f - f_{RF})^2 + (\Gamma_B/2)^2}, \quad (8)$$

in which L is the length of the HNLF, and l_P is the optical pump power injected into the HNLF.

Then, the optical signals shown in Fig. 2(d) are detected by a photodetector (PD). At the output of the PD, the photocurrent of the IF signal down-converted from the desired RF signal is given by

$$i_1(t) = \{4C_1\left[J_0(m_{LO}) + \cos(\theta)\right] + 2(C_2 + C_3)$$
$$\times \left[J_0(m_{LO})\cos(\varphi_1) + \cos(\varphi_1 - \theta)\right]\} \times \cos\left[2\pi(f_{RF} - f_{LO})t\right]$$
$$- \{2(C_2 - C_3)\left[J_0(m_{LO})\sin(\varphi_1) + \sin(\varphi_1 - \theta)\right]\} \times \sin\left[2\pi(f_{RF} - f_{LO})t\right], \quad (9)$$

where φ_1, C_1, C_2, and C_3 are expressed as

$$\varphi_1 = \varphi(f_{RF}) - \varphi(f_{LO}), \quad (10)$$
$$C_1 = -\Re P_{in} t_1 t_2/4 \times J_0(m_{RF})J_0(m_{IM})J_0(m_{IM})J_1(m_{RF})J_1(m_{LO}), \quad (11)$$
$$C_2 = \Re P_{in} t_1 t_2/4 \times G(f_{LO})\,G(f_{RF})\,J_0(m_{RF})J_0(m_{IM})J_0(m_{IM})J_1(m_{RF})J_1(m_{LO}), \quad (12)$$
$$C_3 = \Re P_{in} t_1 t_2/4 \times A(f_{LO})\,A(f_{RF})\,J_0(m_{RF})J_0(m_{IM})J_0(m_{IM})J_1(m_{RF})J_1(m_{LO}), \quad (13)$$

in which $\Re$ is the PD responsivity. Meanwhile, the photocurrent of the IF signal down-converted from the image is given by

$$i_2(t) = \{4C_4\left[J_0(m_{LO}) + \cos(\theta)\right] + 2(C_5 + C_6)$$
$$\times \left[J_0(m_{LO})\cos(\varphi_2) + \cos(\varphi_2 + \theta)\right]\} \times \cos\left[2\pi(f_{LO} - f_{IM})t\right]$$
$$- \{2(C_5 - C_6)\left[J_0(m_{LO})\sin(\varphi_2) + \sin(\varphi_2 + \theta)\right]\} \times \sin\left[2\pi(f_{LO} - f_{IM})t\right], \quad (14)$$

where φ_2, C_4, C_5, and C_6 are expressed as

$$\varphi_2 = \varphi(f_{LO}) - \varphi(f_{IM}), \quad (15)$$
$$C_4 = -\Re P_{in} t_1 t_2/4 \times J_0(m_{RF})J_0(m_{IM})J_0(m_{RF})J_1(m_{IM})J_1(m_{LO}), \quad (16)$$
$$C_5 = \Re P_{in} t_1 t_2/4 \times G(f_{LO})\,G(f_{IM})\,J_0(m_{RF})J_0(m_{IM})J_0(m_{RF})J_1(m_{IM})J_1(m_{LO}), \quad (17)$$
$$C_6 = \Re P_{in} t_1 t_2/4 \times A(f_{LO})\,A(f_{IM})\,J_0(m_{RF})J_0(m_{IM})J_0(m_{RF})J_1(m_{IM})J_1(m_{LO}). \quad (18)$$

The detected signals are then amplified by an electrical amplifier (EA). Thus, the electrical power of the IF signal down-converted from the desired RF signal is given by

$$P_1 = G_A Z_o \times \Big\{\left[4C_1\left[J_0(m_{LO}) + \cos(\theta)\right] + 2(C_2 + C_3)\left[J_0(m_{LO})\cos(\varphi_1) + \cos(\varphi_1 - \theta)\right]\right]^2$$
$$+ \left[2(C_2 - C_3)\left[J_0(m_{LO})\sin(\varphi_1) + \sin(\varphi_1 - \theta)\right]\right]^2\Big\}, \quad (19)$$

TABLE 1
Parameters Adopted for Simulations

Parameter	Value	Unit	Parameter	Value	Unit
P_{in}	9.6	dBm	Γ_B	30	MHz
t_1	6.4	dB	v_B	9.2	GHz
$m_{RF,IM}$	0.19		$\Re$	0.65	A/W
t_2	7.9	dB	Z_o	50	Ω
m_{LO}	0.14		G_A	22	dB
θ	1.5π	rad			

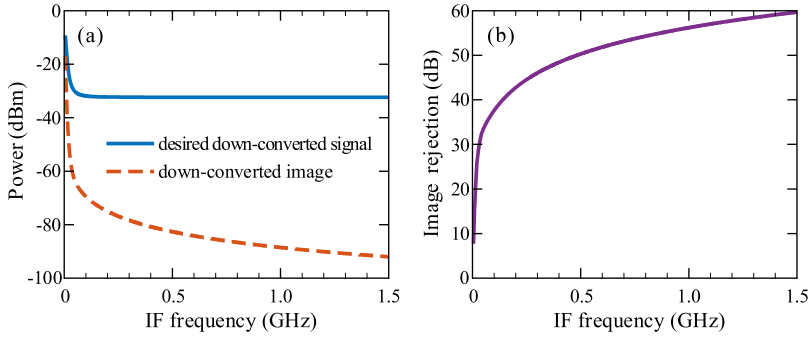

Fig. 3. Simulation results. (a) Calculated IF signal power and (b) the corresponding image rejection versus the IF frequency when the central SBS gain $|G(f_{RF})|^2$ is 25 dB.

and the electrical power of the IF signal down-converted from the image is given by

$$P_2 = G_A Z_o \times \left\{ [4C_4 [J_0(m_{LO}) + \cos(\theta)] + 2(C_5 + C_6)[J_0(m_{LO})\cos(\varphi_2) + \cos(\varphi_2 + \theta)]]^2 \right.$$
$$\left. + [2(C_5 - C_6)[J_0(m_{LO})\sin(\varphi_2) + \sin(\varphi_2 + \theta)]]^2 \right\}, \quad (20)$$

where G_A is the gain of the EA, and Z_o is the PD load resistance. According to (19) and (20), the image rejection ratio (IRR) of the proposed microwave photonic image-reject mixer is written as

$$IRR = 10 \times \log_{10}(P_1/P_2). \quad (21)$$

To illustrate the operation principle of the proposed microwave photonic image-reject mixer, we first consider the case when no pump light is injected into the HNLF, i.e., $I_P = 0$. Substituting $I_P = 0$ into (6)–(8), we find that $G(f) = 1$, $A(f) = 1$, and $\varphi(f) = 0$. By substituting these results into (9)–(13) and (14)–(18), we can conclude that both i_1 and i_2 are equal to 0. This means that in this case, neither the IF signal down-converted from the desired RF signal nor the IF signal down-converted from the image can be obtained.

Then, we consider the case when the pump light is injected into the HNLF. In this case, the +1st-order sidebands of the phase-modulated optical signal are amplified and the −1st-oredr sidebands are attenuated, and therefore a down-converted signal can be obtained at the PD output [19]. To investigate the down-converted signal power and the corresponding image rejection, simulations based on (19)–(21) are carried out. Parameters adopted for simulations are listed in Table 1. Additionally, the frequency of the desired RF signal is fixed at 7.8 GHz and the LO frequency is tuned from 7.795 to 6.300 GHz, thus the IF frequency varies from 5 MHz to 1.5 GHz. Fig. 3(a) shows the calculated IF signal power versus the IF frequency when the central SBS gain $|G(f_{RF})|^2$ is 25 dB, and the corresponding image rejection is shown in Fig. 3(b). In Fig. 3(a), it can be found that when the IF frequency varies from 5 MHz to 1.5 GHz, the IF signal down-converted from the desired RF signal first shows a power decrease and then maintains a power level of about −32 dBm, while the IF signal down-converted from the image suffers a continuous power decrease. Thus, the higher

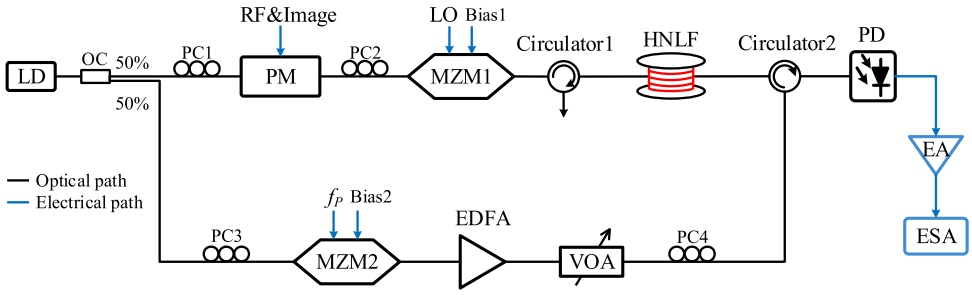

Fig. 4. Experimental setup of the proposed microwave photonic image-reject mixer. LD: laser diode; OC: optical coupler; PC: polarization controller; PM: phase modulator; RF: radio frequency; MZM: Mach-Zehnder modulator; LO: local oscillator; HNLF: high-nonlinear fiber; EDFA: erbium-doped fiber amplifier; VOA: variable optical attenuator; PD: photodetector; EA: electrical amplifier; ESA: electrical spectrum analyzer.

the IF frequency, the larger the image rejection, and an image rejection of larger than 40 dB can be obtained when the IF frequency is higher than 0.2 GHz, as shown in Fig. 3(b).

In summary, when the pump light is injected into the HNLF and the IF frequency is properly chosen, the +1st-order sideband of the desired RF signal is strongly amplified and the −1st-order sideband suffers a significant loss during the SBS process. Thus, the phase-modulated desired RF signal is converted into an intensity-modulated signal. Meanwhile, the LO and image sidebands are only slightly affected by the SBS, and therefore the LO and image signal remain intensity and phase modulation format, respectively. At the PD output, the desired down-converted signal can be obtained and the down-converted image is eliminated, as shown in Fig. 2(e). Thus, the desired signal selection and image rejection are realized by using an SBS-based MPF. In the schematic diagram as illustrated in Fig. 2(a), the configuration without MZM1 acts as such a tunable SBS-based MPF, and the central frequency of the MPF is equal to $f_P - \nu_B$ [19].

3. Experimental Results and Discussions

Experiments based on the setup shown in Fig. 4 are carried out to verify the theoretical analysis. A CW light at 1550.096 nm is emitted from a LD (Koheras BasiK E15) with an optical output power of 12.6 dBm. The CW light is split into two paths via a 50:50 optical coupler. In the upper path, the CW light is injected into the PM (EOSPACE, PM-DV5-40) via PC1. The PM is driven by a RF signal that is generated by an arbitrary waveform generator (AWG, Keysight, M8195A). The phase-modulated optical signal is then injected into MZM1 (Fujitsu, FTM7937EZ) via PC2. The dc bias voltage applied to the MZM1 is 7 V, and the LO generated by the AWG is applied to one arm of the MZM1. Then, the phase- and intensity-modulated optical signals are coupled into a 1.20-km HNLF via circulator1 and interact with the pump light. In the lower path, the CW light is launched into the MZM2 (Fujitsu, FTM7938EZ) via PC3. The MZM2 is biased at its minimum transmission point and driven by a pump tone, which is generated by the AWG and amplified by an EA (CENTELLAX, OA4MVM3). At the output of the MZM2, a carrier-suppressed double sideband (CS-DSB) signal is generated. The optical power of the CS-DSB signal is adjusted by the erbium-doped fiber amplifier (EDFA) and variable optical attenuator (VOA). Then, the CS-DSB signal is injected into the HNLF via circulator2 and acts as the pump light. PC4 is used to align the polarization state of the counter-propagating pump light with the forward-propagating optical signals [22]. After the SBS process, the optical signals are detected by a PD (u^2t, XPDV2120RA) with a bandwidth of 40 GHz. The beating signals are amplified by an EA (SHF, S804 A) and measured by an electrical spectrum analyzer (ESA, Keysight, N9030A).

First, the frequencies of the desired RF and LO signals are set to 7.8 and 7.3 GHz, respectively. Because the Brillouin frequency shift of the HNLF is 9.2 GHz, the frequency of the pump tone is set to 17 GHz. The RF signal power applied to the PM is −7.03 dBm, and the LO power applied to MZM1 is −10.66 dBm. Fig. 5(a) and (b) show the measured optical spectra of the pump light

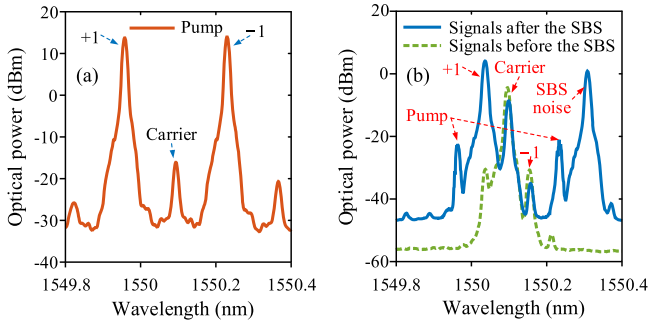

Fig. 5. Optical spectra of (a) the pump light injected into the HNLF, and (b) optical signals before (green dash line) and after (blue solid line) the SBS process.

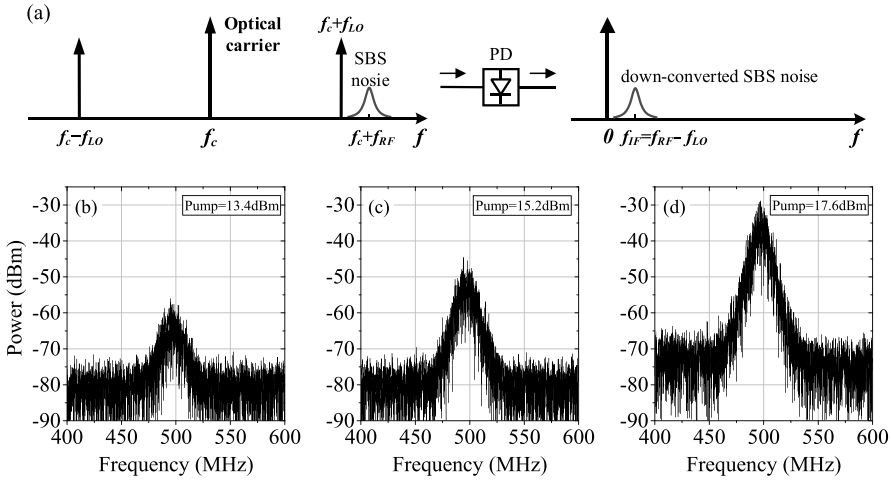

Fig. 6. SBS noise. (a) When no electrical signal is applied to the PM, schematic diagram of the optical spectra before the PD and electrical spectra at the PD output. Measured electrical spectra of the down-converted SBS noise when the optical pump power is (a) 13.4, (b) 15.2, and (c) 17.6 dBm.

and optical signals respectively, when the optical pump power is 15.2 dBm. As can be observed, in Fig. 5(a), the optical carrier power is suppressed to −16 dBm, which is 30 dB lower than the ±1st-order sidebands power. In Fig. 5(b), it can be found that after interacting with the pump light, the +1st-order sidebands of the optical signals are amplified, and the −1st-order sidebands of the optical signals are attenuated. Additionally, it can be observed the SBS noise generated by the −1st-order sideband of the pump light is at a high power level, which indicates that when no electrical signal is applied to the PM, a SBS noise generated by the +1st-order sideband of the pump light still exits at $f_c + f_{RF}$. After photodetection, the SBS noise is down-converted to the IF band, as shown in Fig. 6(a). Fig. 6(b)—(d) show the measured electrical spectra of the down-converted SBS noise when the optical pump power is 13.4, 15.2, and 17.6 dBm, respectively. It is observed that the down-converted SBS noise power increases quickly as the optical pump power is increased. To reduce the SBS noise, the optical pump power is set to 13.4 dBm in the following experiments.

Once the optical pump power is fixed, the dc bias voltage and LO power applied to MZM1 can be also optimized to maintain high image rejection. To choose an optimum dc bias voltage, the frequencies and power of the microwave signals including the desired RF signal, LO and pump tone remain the same, and the dc bias voltage is tuned from 0 to 10 V. Fig. 7(a) shows the measured image rejection versus the dc bias voltage applied to MZM1, and the corresponding IF signal power is shown in Fig. 7(b). Inset in Fig. 7(a) shows the measured normalized transmission of the MZM1 versus the bias voltage. It is observed that when the dc bias voltage is 7 V, the image rejection gets its maximal value and the corresponding desired down-converted signal power almost reaches

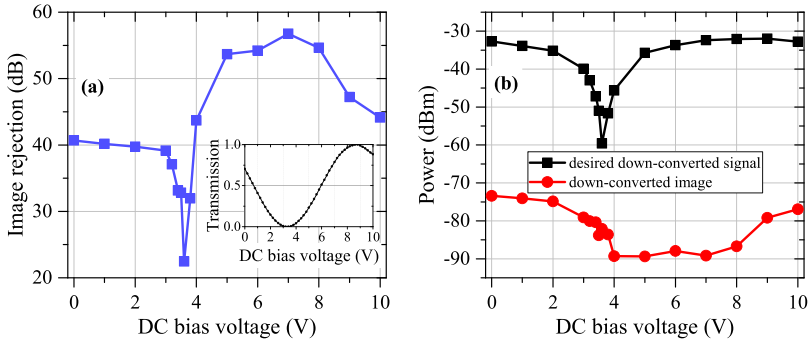

Fig. 7. (a) Measured image rejection and (b) the corresponding IF signal power versus the dc bias voltage applied to MZM1. Inset in (a) shows the measured normalized transmission of the MZM1 versus the dc bias voltage.

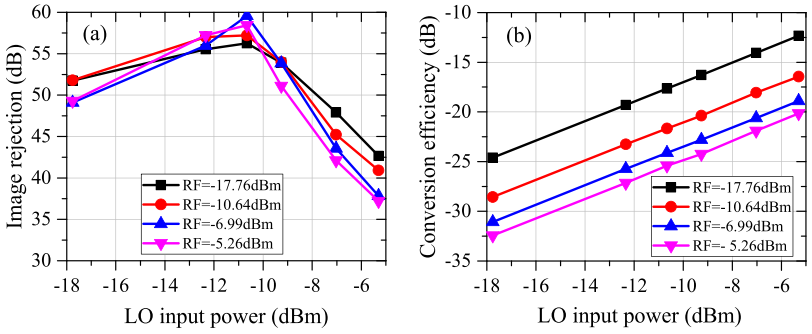

Fig. 8. (a) Measured image rejection and (b) conversion efficiency with different LO and RF input power.

its maximum power level, as shown in Fig. 7(a) and (b), respectively. Therefore, in the following experiments, the dc bias voltage applied to MZM1 is set to 7 V to achieve both high image rejection and relatively high conversion efficiency (approximately −22 dB).

Then, to determine the LO power applied to MZM1, the frequencies of the microwave signals including the desired RF signal, LO and pump tone still remain the same, while the LO power applied to the MZM1 varies from −17.76 to −5.30 dBm, and the RF power applied to the PM is set to −17.76, −10.64, −6.99, and −5.26 dBm, respectively. Fig. 8(a) shows the measured image rejection with different LO and RF input power, and the corresponding conversion efficiency, which is defined as the ratio of the desired IF output power to the desired RF input power, is shown in Fig. 8(b). In Fig. 8(a), an image rejection of larger than 40 dB is achieved when the LO input power is lower than −7 dBm. Additionally, when the RF input power varies from −17.76 to −5.26 dBm, the fluctuation of the image rejection is less than 6 dB. In Fig. 8(b), it is observed that the conversion efficiency decreases as the RF input power is increased. This is because the pump is depleted when the seed signal (i.e., the +1st-order sideband of the desired RF signal) power is high, which causes Brillouin gain saturation [21]. Additionally, a high LO input power can improve conversion efficiency. In experiment, a high image rejection is the primary consideration, and therefore the LO power applied to MZM1 is set to −10.66 dBm according to the measured results in Fig. 8(a). Correspondingly, when the LO power is −10.66 dBm and the RF power is −10.64 dBm, the conversion efficiency is −22 dB, which is higher than the result (−30 dB) in [14].

Next, the image rejection across a wide IF and RF band is experimentally demonstrated. In this part, the RF signal power applied to the PM is set to −7.03 dBm, and the LO power applied to the MZM1 is −10.66 dBm. To verify the image rejection across a wide IF band, the frequency of the desired RF signal is set to 7.8 GHz, and the LO frequency is tuned from 7.79 to 6.30 GHz so that the IF frequency varies from 0.01 to 1.5 GHz. The measured IF signal power versus the IF frequency is shown in Fig. 9(a), and the corresponding image rejection is shown in Fig. 9(b). Compared

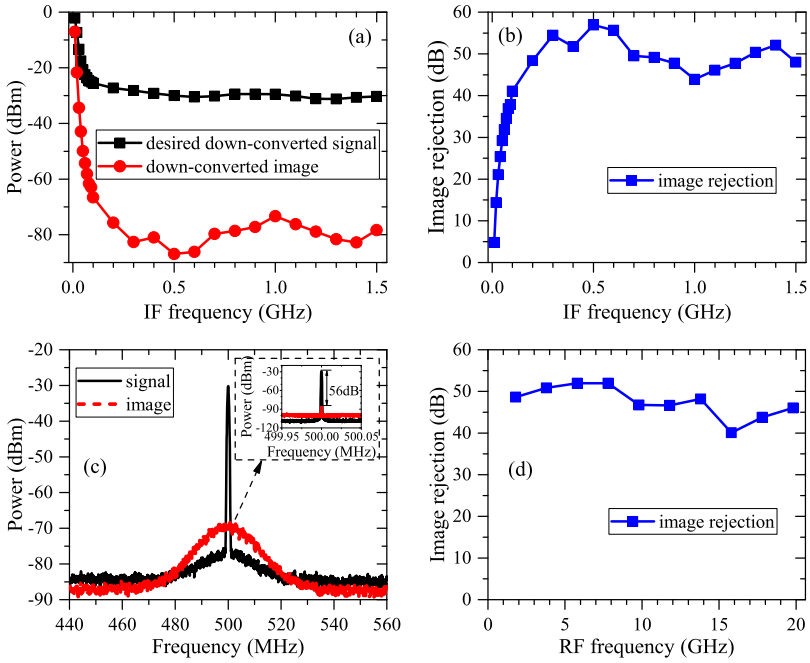

Fig. 9. Image rejection across a wide IF/RF band. (a) Measured IF signal power and (b) the corresponding image rejection versus the IF frequency. (c) Measured electrical spectra of the desired down-converted signal and down-converted image. (d) Measured image rejection across a wide RF band when the IF frequency is fixed at 0.5 GHz.

with the simulation results in Fig. 3(a), the variations of the measured IF signal power in Fig. 9(a) are basically consistent with the results in Fig. 3(a), except when the IF frequency is higher than 0.2 GHz, the measured electrical power of the down-converted image fluctuates around −80 dBm instead of keeping decrease like Fig. 3(a). This is caused by the down-converted SBS noise, which is not considered in the simulation. In Fig. 9(b), it can be observed that an image rejection of larger than 40 dB is obtained across a wide IF band of 0.2–1.5 GHz. Fig. 9(c) shows the measured electrical spectra of the desired down-converted signal and down-converted image when the LO frequency is 7.3 GHz. As can be seen, the down-converted image is rejected by 56 dB. In addition, the noise in the electrical spectrum of the down-converted image is at a higher power level than the noise in the electrical spectrum of the desired down-converted signal. This is because more optical pump power is converted to SBS noise when the seed signal, i.e., the +1st-order sideband of the desired RF signal, is absent [23]. Then, in order to investigate the image rejection across a wide RF band, the frequency of the desired RF signal is tuned from 1.8 to 19.8 GHz and the LO frequency is tuned from 1.3 to 19.3 GHz, thus the IF frequency is maintained at 0.5 GHz. Correspondingly, the frequency of the pump tone is tuned from 11 to 29 GHz. The measured image rejection across a wide RF band is shown in Fig. 9(d). It can be observed that the image is rejected by more than 40 dB when the RF frequency varies from 1.8 to 19.8 GHz.

Furthermore, the structure of the proposed mixer is not complicated compared to previously reported mixers based on Hartley architecture [10]–[14] and electrical filter [16], [17]. For example, in [10], when the RF frequency is changed, an extra tunable delay line and VOA must be employed and adjusted accordingly to compensate for the phase and amplitude imbalance of the optical/electrical coupler. Otherwise, the image rejection degrades to 28.4 dB [10]. To the best of our knowledge, this is the first demonstration of an MPF-based microwave photonic image-reject mixer, and the achieved image rejection ratio is comparable to some of the previously reported mixers [10], [14], for example, about 40 dB in [14].

4. Conclusion

A flexible microwave photonic image-reject mixer has been theoretically and experimentally demonstrated. The mixer is implemented with a widely tunable MPF based on SBS and an MZM driven by the LO. By adjusting the central frequency of the SBS-based MPF, the desired RF signal is exactly pre-selected and down-converted to an IF signal with the image eliminated. Experimental results exhibit an image rejection of larger than 40 dB across a wide IF band of 0.2—1.5 GHz. Meanwhile, when the frequency of the desired RF signal is tuned from 1.8 to 19.8 GHz, the image rejection still remains above 40 dB.

References

[1] S. A. Maas, *Microwave Mixers*. Norwood, MA, USA: Artech House, 1993.
[2] G. K. Gopalakrishnan, W. K. Burns, and C. H. Bulmer, "Microwave-optical mixing in LiNbO3 modulators," *IEEE Trans. Microw. Theory Techn.*, vol. 41, no. 12, pp. 2383–2391, Dec. 1993.
[3] Z. S. Jia, J. J. Yu, and G. K. Chang, "All-optical 16 × 2.5 Gb/s WDM signal simultaneous up-conversion based on XPM in an NOLM in ROF systems," *IEEE Photon. Technol. Lett.*, vol. 17, no. 12, pp. 2724–2726, Dec. 2005.
[4] J. Yu, Z. Jia, L. Yi, and Y. Su, "Optical millimeter-wave generation or up-conversion using external modulators," *IEEE Photon. Technol. Lett.*, vol. 18, no. 1, pp. 265–267, Jan. 2006.
[5] E. H. W. Chan and R. A. Minasian, "Microwave photonic downconverter with high conversion efficiency," *J. Lightw. Technol.*, vol. 30, no. 23, pp. 3580–3585, Dec. 2012.
[6] Y. K. Seo, C. S. Choi, and W. Y. Choi, "All-optical signal up-conversion for radio-on-fiber applications using cross-gain modulation in semiconductor optical amplifiers," *IEEE Photon. Technol. Lett.*, vol. 14, no. 10, pp. 1448–1450, Oct. 2002.
[7] H. J. Song, J. S. Lee, and J. I. Song, "Signal up-conversion by using a cross-phase-modulation in all-optical SOA-MZI wavelength converter," *IEEE Photon. Technol. Lett.*, vol. 16, no. 2, pp. 593–595, Feb. 2004.
[8] Z. Jia, J. Yu, and G.-K. Chang, "A full-duplex radio-over-fiber system based on optical carrier suppression and reuse," *IEEE Photon. Technol. Lett.*, vol. 18, no. 16, pp. 1726–1728, Aug. 2006.
[9] L. Chao, C. Wenyue, and J. F. Shiang, "Photonic mixers and image-rejection mixers for optical SCM systems," *IEEE Trans. Microw. Theory Techn.*, vol. 45, no. 8, pp. 1478–1480, Aug. 1997.
[10] J. Zhang, E. H. W. Chan, X. Wang, X. Feng, and B. Guan, "High conversion efficiency photonic microwave mixer with image rejection capability," *IEEE Photon. J.*, vol. 8, no. 4, Aug. 2016, Art. no. 3900411.
[11] Z. Z. Tang and S. L. Pan, "Image-reject mixer with large suppression of mixing spurs based on a photonic microwave phase shifter," *J. Lightw. Technol.*, vol. 34, no. 20, pp. 4729–4735, Oct. 2016.
[12] Y. Gao, A. Wen, W. Chen, and X. Li, "All-optical, ultra-wideband microwave I/Q mixer and image-reject frequency down-converter," *Opt. Lett.*, vol. 42, no. 6, pp. 1105–1108, Mar. 2017.
[13] P. X. Li, W. Pan, X. H. Zou, B. Lu, L. S. Yan, and B. Luo, "Image-free microwave photonic down-conversion approach for fiber-optic antenna remoting," *IEEE J. Quantum Electron.*, vol. 53, no. 4, Aug. 2017, Art. no. 9100208.
[14] Z. Tang and S. Pan, "Reconfigurable microwave photonic mixer with minimized path separation and large suppression of mixing spurs," *Opt. Lett.*, vol. 42, no. 1, pp. 33–36, Jan. 2017.
[15] S. Wu and B. Razavi, "A 900-MHz/1.8-GHz CMOS receiver for dual-band applications," *IEEE J. Solid-State Circuits*, vol. 33, no. 12, pp. 2178–2185, Dec. 1998.
[16] A. Ward, L. T. Nichols, P. D. Biernacki, and K. J. Williams, "An ultrawideband image rejecting microwave downconverter using WDM," in *Proc. IEEE Int. Topical Meeting Microw. Photon.*, 1999, vol. 1, pp. 239–242.
[17] S. J. Strutz, P. Biernacki, L. Nichols, and K. J. Williams, "Demonstration of a wide-band image rejection microwave downconverter," *IEEE Photon. Technol. Lett.*, vol. 12, no. 6, pp. 687–689, Jun. 2000.
[18] H. T. Tang, Y. Yu, C. Zhang, Z. W. Wang, L. Xu, and X. L. Zhang, "Analysis of performance optimization for a microwave photonic filter based on stimulated Brillouin scattering," *J. Lightw. Technol.*, vol. 35, no. 20, pp. 4375–4383, Oct. 2017.
[19] W. Zhang and R. A. Minasian, "Widely tunable single-passband microwave photonic filter based on stimulated Brillouin scattering," *IEEE Photon. Technol. Lett.*, vol. 23, no. 23, pp. 1775–1777, Dec. 2011.
[20] A. Choudhary *et al.*, "Tailoring of the Brillouin gain for on-chip widely tunable and reconfigurable broadband microwave photonic filters," *Opt. Lett.*, vol. 41, no. 3, pp. 436–439, Feb. 2016.
[21] R. W. Boyd, *Nonlinear Optics*. New York, NY, USA: Academic, 2003.
[22] M. O. Van Deventer and A. J. Boot, "Polarization properties of stimulated Brillouin scattering in single-mode fibers," *J. Lightw. Technol.*, vol. 12, no. 4, pp. 585–590, Apr. 1994.
[23] X. S. Yao, "Brillouin selective sideband amplification of microwave photonic signals," *IEEE Photon. Technol. Lett.*, vol. 10, no. 1, pp. 138–140, Jan. 1998.